crystals

Article

# Very High Cycle Fatigue Damage of TC21 Titanium Alloy under High/Low Two-Step Stress Loading

**Baohua Nie [1], Shuai Liu [1], Yue Wu [1], Yu Song [1], Haiying Qi [1], Binqing Shi [1], Zihua Zhao [2,*] and Dongchu Chen [1,*]**

[1] School of Materials Science and Hydrogen Energy, Foshan University, Foshan 528000, China
[2] School of Materials Science and Engineering, Beihang University, Beijing 100191, China
* Correspondence: zhzh@buaa.edu.cn (Z.Z.); chendc@fosu.edu.cn (D.C.); Tel.: +86-010-8233-3264 (Z.Z.); +86-075-7827-00525 (D.C.)

**Abstract:** Very high cycle fatigue (VHCF) tests were carried out under variable amplitude loading for TC21 titanium alloy. The first level of high amplitude loading was set as 950 MPa close to yield strength, and the second level of low amplitude loading was determined between 435 MPa and 500 MPa where fatigue cracks initiated at the specimen subsurface under constant amplitude. The results indicate that the high/low stress block significantly reduced the cumulative fatigue life of low stress amplitude, and the fatigue crack initiation site changed from the specimen subsurface under constant loading to the specimen surface under stress block. Based on continuum damage mechanics, the fatigue damage model of two-step stress block was established to estimate the fatigue damage process. The prediction of cumulative fatigue life generally agreed with the experimental data. The cumulative fatigue damage of the stress block was related to the stress amplitude and the cycle ratio, which determined the stress fatigue damage and its interaction damage. The surface crack initiation in the stress block accelerated fatigue damage of low stress amplitude, reducing the cumulative life.

**Keywords:** VHCF; variable amplitude; fatigue damage; titanium alloy



**Citation:** Nie, B.; Liu, S.; Wu, Y.; Song, Y.; Qi, H.; Shi, B.; Zhao, Z.; Chen, D. Very High Cycle Fatigue Damage of TC21 Titanium Alloy under High/Low Two-Step Stress Loading. *Crystals* **2023**, *13*, 139. https://doi.org/10.3390/cryst13010139

Academic Editors: Peng Chen, Feng Shi and Xiao-Wu Li

Received: 6 December 2022
Revised: 5 January 2023
Accepted: 10 January 2023
Published: 13 January 2023



## 1. Introduction

Titanium alloys were widely used in key aerospace components due to their high strength, toughness, and corrosion resistance [1]. Fatigue performance was the key factor of reliability service for key components [2,3]. In the ultra-long service process, these key components withstood high frequency vibration alternating load, where the cyclic number was beyond $10^7$ cycles, and very high cycle fatigue (VHCF) of key components was of great concern [4,5]. In fact, key components often underwent variable amplitude loading (VA). Compared with the constant amplitude loading (CA), VHCF behavior of high-strength titanium alloy under variable amplitude should be further investigated, providing the guidance for high reliability service of key aviation components.

In recent years, the very high cycle fatigue of titanium alloys attracted the attention of researchers. VHCF properties and damage mechanisms, etc., involving the material microstructure [6], temperature [7], and stress ratio [8,9], were systematically studied. However, there were few reports on the research of the very high cycle fatigue of titanium alloys under variable amplitude. Based on a Gauss distribution of stress amplitudes, Mayer et al. [10–13] investigated the variable amplitude VHCF behavior of the 2024 aluminum alloy and high-strength steels. They found that the VHCF crack initiated at the specimen surface under variable amplitude for 2024 aluminum alloy. The cumulative damage sum decreased as fatigue life increased from high cycle fatigue (HCF) to VHCF, which was significantly related to the stress ratio [10,11]. For high-strength steel [12,13], VHCF under variable amplitude displayed the similar crack initiation laws to that under constant amplitude, and suggested that fatigue damage should be analyzed for surface and internal initiation, respectively.

On the other hand, the initiation mechanism of VHCF for high-strength materials was investigated by using two-stage stress blocks. The growth rate of the fine granular area (FGA) at the crack initiation site of VHCF was quantitatively estimated by the tree ring feature marked by the two-stage stress [14–18]. Under variable amplitude loading, the delay and acceleration of microcracks resulted in greater roughness in the FGA region [19,20]. By using similar two-stage stress blocks, Zhao et al. [21] investigated the microcrack propagation behavior in FGA around the porosity of an electron beam-welded joint for high-strength titanium alloy.

However, little attention was paid to the effect of high stress amplitude with a few cycles in the service life. The effect of low cycle fatigue (LCF) predamage on subsequent VHCF properties was investigated for TC21 titanium alloy [22,23] and A42 steel [24,25]. VHCF damage models combined with LCF predamage were, respectively, established by Lemaitre damage mechanics [23] and Chaboche damage mechanics [24,25]. However, the interaction between high and low stress amplitude was not considered, which was significant for various amplitude fatigue.

In this paper, VHCF properties and crack initiation characteristics under high/low two-step stress loading for TC21 titanium alloy was investigated. The fatigue damage model under high/low two-step stress loading was established based on Lemaitre damage theory to discuss the interaction between high and low stress amplitude, providing valuable guidance for the engineering application of high-strength titanium alloys subjected to variable loading.

## 2. Experimental Procedures

### 2.1. Materials

TC21 titanium alloy with its nominal composition of Ti-6Al-2Zr-2Sn-2Mo-2Nb-1.5Cr (wt.%) was used in this work. The alloys with basketweave microstructure obtained a tensile strength of 1070 MPa [26] and a very high cycle fatigue limit of 430 MPa [22], respectively.

### 2.2. Constant Amplitude Fatigue

Constant amplitude fatigue tests were carried out by an ultrasonic fatigue test machine (SHIMADZU, Kyoto, Japan) at a load ratio of R = −1, which was an accelerating testing method with a 20 kHz frequency [27]. The specimen geometry was designed based on the elastic wave theory. The geometries and dimensions of the fatigue specimens are illustrated in Figure 1.

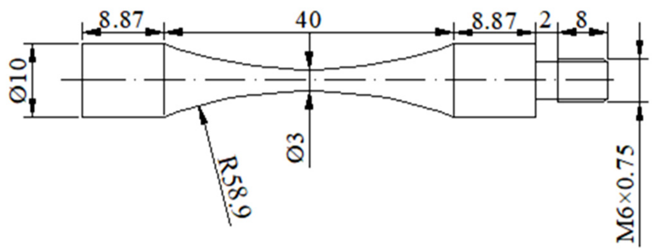


**Figure 1.** Geometries and dimensions of the test specimens (in mm).

### 2.3. Variable Amplitude Fatigue

Variable amplitude fatigue was applied by a repeated high/low two-step loading procedure, which started from a high stress block $\sigma_H$, and then was followed by a low stress block $\sigma_L$ (Figure 2). High stress fatigue was carried out for ultrasonic specimens by a hydraulic fatigue machine (Instron 8801, Instron Company, Boston, MA, USA), and low stress fatigue was tested by an ultrasonic fatigue machine (SHIMADZU, Kyoto, Japan). Both high stress and low stress fatigue were at a load ratio of R = −1.

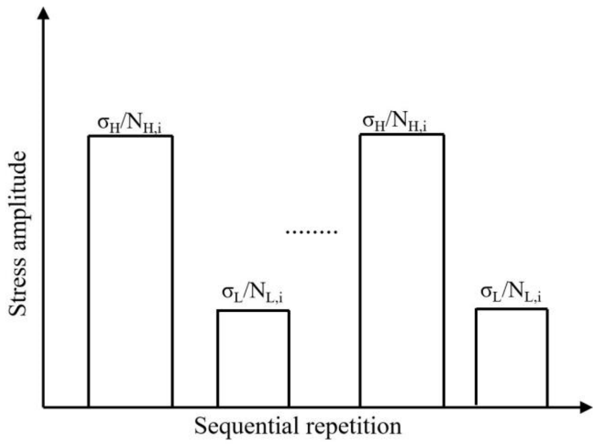


**Figure 2.** Repeated high/low two-step loading procedure.

According to the previous investigation [22], surface cracks of TC21 titanium alloy were not observed under a 950 MPa stress amplitude with 5% of the expected life (90 cycles), thus the cycle number of high stress block $N_{H,i}$ was selected as 10 cycles. The low stress block was set as 430 MPa, 450 MPa, 480 MPa, and 500 MPa, respectively, where fatigue cracks initiated at the specimen subsurface under constant amplitude. The corresponding constant amplitude fatigue life was from $2 \times 10^6$ cycles to $2.6 \times 10^7$ cycles, thus the cycle number of low stress block $N_{L,i}$ was, respectively, determined as $2 \times 10^4$ cycles and $2 \times 10^5$ cycles to investigate the effect of the cycle ratio. Four parallel experiments were conducted for each group of experiments, and the average value was taken as fatigue life.

## 3. Results and Discussion

### *3.1. Variable Amplitude Fatigue Behavior*

Figure 3 shows fatigue life S-N curves of TC21 titanium alloy under constant amplitude and variable amplitude loading. As for constant amplitude fatigue, there was a transition stress of 540 MPa between surface initiation and subsurface initiation. Above the transition stress, fatigue cracks were initiated at the specimen surface, while fatigue cracks were initiated at the specimen subsurface below the transition stress. However, fatigue cracks were initiated at the specimen surface under stress blocks.

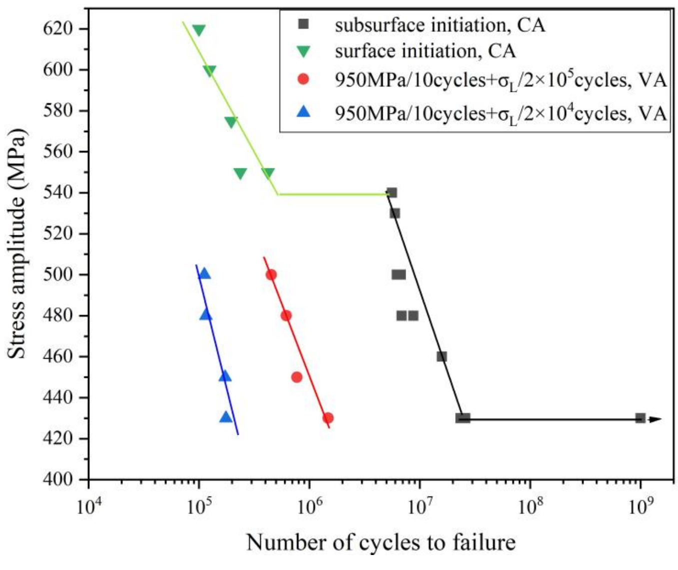


**Figure 3.** S-N curves under constant and variable amplitude loading for TC21 alloy (arrows denote the run-out specimens).

For variable amplitude fatigue, a small amount of high stress amplitude loading in the stress block significantly reduced fatigue life at low stress amplitude. The cumulative cycles increased with the decrease in the second low stress amplitude, and were far lower than that under constant amplitude. Furthermore, the cumulative cycles under low amplitude with $2 \times 10^4$ cycles were lower than that with $2 \times 10^5$ cycles. Compared to the second level of $2 \times 10^5$ cycles, the number of cycle blocks with the second stress for $2 \times 10^4$ cycles were increased, but the cumulative life of low stress amplitude decreased.

According to the linear cumulative damage theory [10], fatigue damage of a TC21 titanium alloy stress block was:

$$D_{B,i} = \frac{N_{H,i}(\sigma_H)}{N_{CA}(\sigma_H)} + \frac{N_{L,i}(\sigma_L)}{N_{CA}(\sigma_L)} \tag{1}$$

where $D_{B,i}$ was fatigue damage of the $i$th stress block, and $N_{CA}$ was fatigue life under constant stress amplitude. Fatigue damage of the $i$th stress block $D_{B,i}$ was constant due to the constant amplitude of high and low stress and the constant number of cycles, and the number of stress blocks was: $N = 1/D_{B,\mathrm{i}}$.

For the second level $2 \times 10^5$ cycles, based on the linear cumulative damage theory, the predicted value was non-conservative, at almost 10 times that of the experiment (Table 1). In comparison with fatigue life after LCF predamage under 950 MPa stress amplitude [22], the cumulative life of low stress amplitude was lower than that that of LCF predamage. It indicated that the interaction between high and low stress amplitudes in the stress block accelerated fatigue damage, and reduced the cumulative life.

**Table 1.** Cumulative life under variable amplitude loading (cycle ratio: $10/2 \times 10^5$).

| Stress $\sigma_H/\sigma_L$, MPa | Experimental Data | Prediction of Linear Cumulative Damage | Prediction of This Damage Model | Prediction Error of this Damage Model | Fatigue Life of Predamage Specimens [22] |
|---|---|---|---|---|---|
| 950/500 | $30/4.54 \times 10^5$ | $286/5.71 \times 10^6$ | $30/4.84 \times 10^5$ | +6.61% | $45/4.8 \times 10^5$ |
| 950/480 | $30/6.2 \times 10^5$ | $324/6.48 \times 10^6$ | $30/5.80 \times 10^5$ | −6.45% | $45/8.0 \times 10^5$ |
| 950/450 | $40/7.74 \times 10^5$ | $555/1.11 \times 10^7$ | $50/8.50 \times 10^5$ | +9.82% | $45/1.7 \times 10^6$ |
| 950/430 | $80/1.48 \times 10^6$ | $715/1.43 \times 10^7$ | $80/1.55 \times 10^6$ | +4.733% | $90/1.5 \times 10^7$ |

For stress blocks with both $2 \times 10^4$ cycles and $2 \times 10^5$ cycles, fatigue cracks were initiated at the specimen surface, and fatigue cracks propagated with the radial fracture surface (Figure 4). VHCF cracks were initiated at the specimen subsurface where the crack initiation site illustrated radial fracture characteristics indicated by red circle in Figure 5a, and the fine granular area was observed at the crack source area (Figure 5b) which was the typical characteristic of VHCF [6,7]. It was inferred that high stress with a few cycles in the stress block promoted the initiation of surface microcracks. However, compared to the predamaged specimens under 950 MPa stress amplitude with 45 cycles, where fatigue crack was initiated at the specimen subsurface under low stress amplitude [22], the interaction of high and low stress accelerated the fatigue damage in the stress block and promoted the specimen surface initiation.

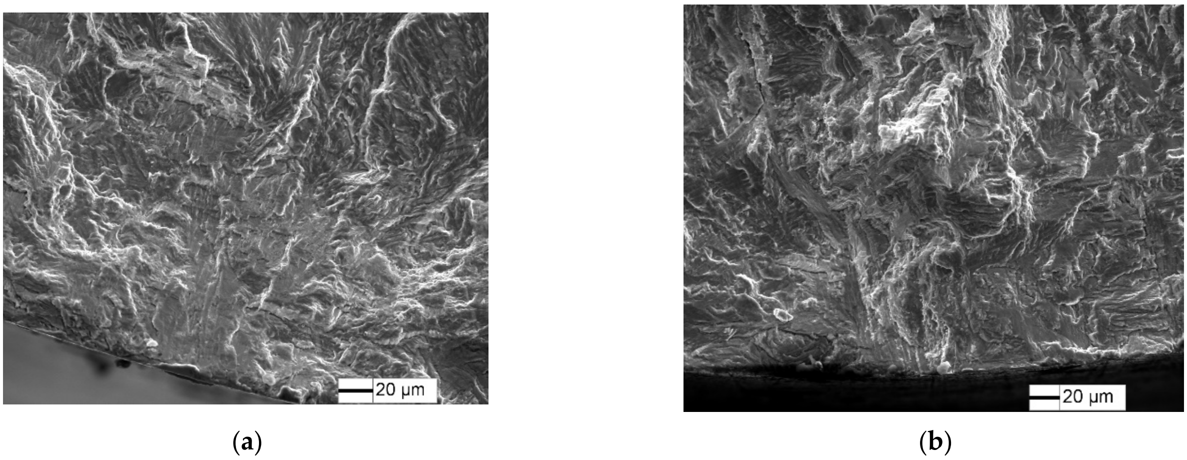


**Figure 4.** Fatigue fracture morphology of TC21 titanium alloy under variable amplitude: (**a**) 950 MPa/10 cycles + 450 MPa/2 × $10^5$ cycles; and (**b**) 950 MPa/10 cycles + 450 MPa/2 × $10^4$ cycles.

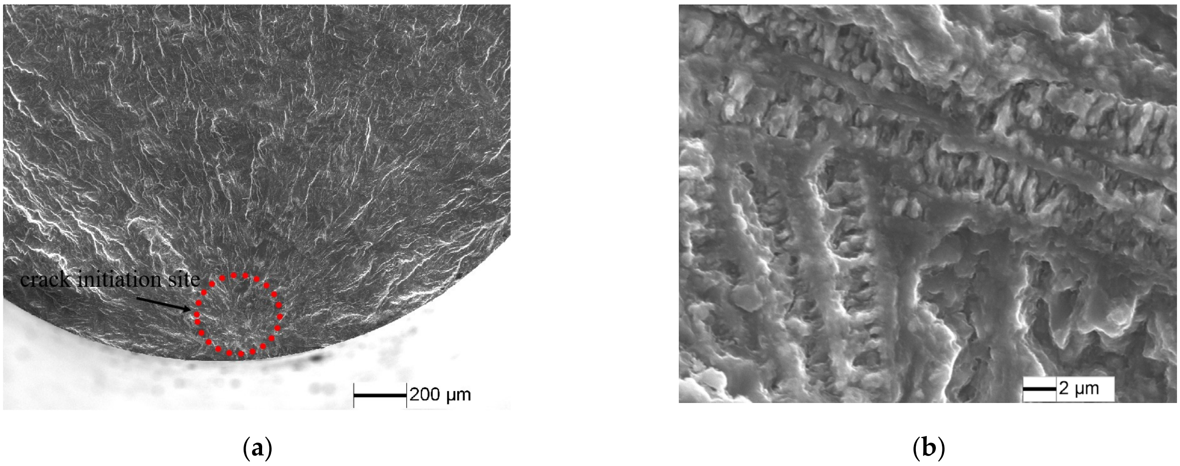


**Figure 5.** Fatigue fracture surface of TC21 titanium alloy at σ = 480 MPa, $N$ = 8.76 × $10^6$ ycles: (**a**) fatigue crack initiation site; and (**b**) high magnification morphology.

*3.2. Continuum Damage of Variable Fatigue*

3.2.1. Fatigue Damage Model

The *i*th stress block contained high stress block $\sigma_H/N_{H,i}$ and low stress block $\sigma_L/N_{L,i}$. According to literature [28], when high stress produced low cycle fatigue damage, fatigue damage $D_{H,i}$ of the *i*th high stress block was expressed as:

$$D_{H,i} = 1 - [(1 - D_{H,i-1})^{\frac{1}{n}+2\alpha} - \frac{4\sigma_H{}^{\frac{1}{n}+2\alpha}}{(2ES)^{\alpha} nk^{1/n}} N_{H,i}]^{\frac{1}{\frac{1}{n}+2\alpha}}. \tag{2}$$

Fatigue life $N_{R,H}$ under high constant amplitude loading was given as [28]:

$$N_{R,H} = [1 - (1 - D_{c,H})^{\frac{1}{n}+2\alpha}] \frac{(2ES)^{\alpha} nk^{1/n}}{4\sigma_H{}^{\frac{1}{n}+2\alpha}} \tag{3}$$

Combined with Formulas (2) and (3), fatigue damage $D_{H,i}$ of the *i*th high stress block was expressed as:

$$D_{H,i} = 1 - [(1 - D_{H,i-1})^{\frac{1}{n}+2\alpha} - [1 - (1 - D_{c,H})^{\frac{1}{n}+2\alpha}] \frac{N_{H,i}}{N_{R,H}}]^{\frac{1}{\frac{1}{n}+2\alpha}} \tag{4}$$

where $k$ and $n$ were the cyclic hardening/softening coefficient and index. $E$ was the elastic modulus of TC21 titanium alloy. The damage strength $S$ represented the amount of fatigue damage produced by each plastic strain increment. The parameter $\alpha$ was the damage nonlinear cumulative coefficient. $D_{c,H}$ was the critical value of high stress fatigue damage.

According to literature [23], as low stress produced VHCF damage, fatigue damage $D_{L,i}$ of the $i$th low stress block was expressed as:

$$D_{L,i} = 1 - [(1 - D_{L,i-1})^{(2s+1)} - \frac{2(R_v^u)^s[(\sigma_L + k\sigma_f)^{2s+1} - [\sigma_f(1+k)]^{2s+1}]}{(2ES)^s C(1+k)^{2s+1}} N_{L,i}]^{\frac{1}{2s+1}} \tag{5}$$

where $R_\nu^\mu$ was triaxial stress state function. The parameter s represented the nonlinear cumulative parameter of fatigue damage, and $\sigma_f$ was VHCF limit. The parameters of $C$ was material constant.

Fatigue life $N_{R,L}$ under low constant amplitude loading was given as [23]:

$$N_{R,L} = [1 - (1 - D_{c,L})^{(2s+1)}] \frac{(2ES)^s k}{2(R_\nu^\mu)^s[(\frac{\sigma_L + C\sigma_f}{1+C})^{2s+1} - \sigma_f{}^{2s+1}]}. \tag{6}$$

Combined with Formulas (5) and (6), fatigue damage $D_{L,i}$ of the $i$th stress block was expressed as:

$$D_{L,i} = 1 - [(1 - D_{L,i-1})^{2s+1} - [1 - (1 - D_{c,L})^{2s+1}] \frac{N_{L,i}}{N_{R,L}}]^{\frac{1}{2s+1}} \tag{7}$$

where $D_{c,L}$ was the critical value of low stress fatigue damage.

As the initial damage value of low stress block $D_{L,i\text{-}1}$, high stress damage $D_{H,i}$ can be equivalent to the low stress damage $\lambda D_{H,i}$. The parameter $\lambda$ was the coefficient of high/low stress damage conversion, and the calculation process of $\lambda$ can infer to the previous paper [23]. Both stress block damage and high stress damage were converted into equivalent fatigue damage at low stress in this paper. Therefore, the $i$th stress block damage $D_{B,i}$ was calculated as:

$$D_{B,i} = 1 - [(1 - \lambda D_{H,i})^{2s+1} - [1 - (1 - D_{c,L})^{2s+1}] \frac{N_{L,i}}{N_{R,L}}]^{\frac{1}{2s+1}}. \tag{8}$$

The initial value of high stress damage in the ($i$ + 1)th stress block was: $D_{L,i+1} = D_{B,i}/\lambda$, which was substituted into Formulas (4), (7) and (8) for cyclic calculation. When the stress block $D_{B,i}$ reached the critical damage value of $D_{c,L}$, fatigue crack was initiated.

The damage of the interaction between high stress amplitude and low stress amplitude $D_{H/L}$ was expressed as:

$$D_{H/L,i} = D_{B,i} - D_{H,i} - D_{L,i}. \tag{9}$$

3.2.2. The Parameters and Validation of Model

The high stress in stress blocks resulted in the crack initiation at the specimen surface, thus the characteristics of surface initiation should be considered for the parameter $s$ in the stress block. The nonlinear fatigue damage parameter $s$ can be expressed as [23]:

$$s = B_0(\frac{\sigma_u - \sigma_a}{\sigma_u - \sigma_f}) \tag{10}$$

where $B_0$ was the adaptive parameter of the fatigue damage accumulation process, and $\sigma_u$ was the tensile strength of TC21 titanium alloy.

According to the Formula (6), by fitting the S-N curve of the undamaged specimens with the numerical iteration calculation (Figure 6), the parameter of $B_0$ was equal to 1.43 for the surface initiation. The parameters of fatigue damage model under variable amplitude are shown in Table 2.

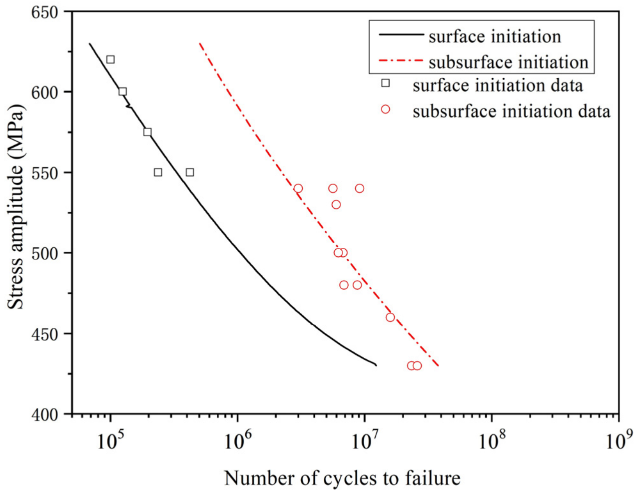


**Figure 6.** Fitting of fatigue damage parameters for the surface initiation.

**Table 2.** The parameters of variable amplitude fatigue damage model.

| *E*/GPa | $\sigma_u$/MPa | $\sigma_f$/MPa | *K*/MPa | *C* | *S*/MPa | $B_0$/Surface | $B_0$/Subsurface | $D_{c,L}$ | $D_{c,H}$ |
|---|---|---|---|---|---|---|---|---|---|
| 110<br>[26] | 1070<br>[26] | 430<br>[23] | 1067.3<br>[26] | 61.84<br>[28] | 130<br>[28] | 1.43<br>fitting | 1.64<br>[23] | 0.62<br>[23] | 1.14<br>[28] |

Based on the fatigue damage model, the cumulative life under different low stress amplitude was predicted with the second level of 2 × $10^5$ cycles (Figure 7). Under the second level stress of 450 MPa, fatigue cumulative life was 950 MPa/50 cycles and 450 MPa/8.5 × $10^5$ cycles, and there was one more stress block than the experimental data. However, the predicted values under other stress amplitudes were close to the experimental data. Thus, the prediction of cumulative life with this model generally agreed with the experimental data.

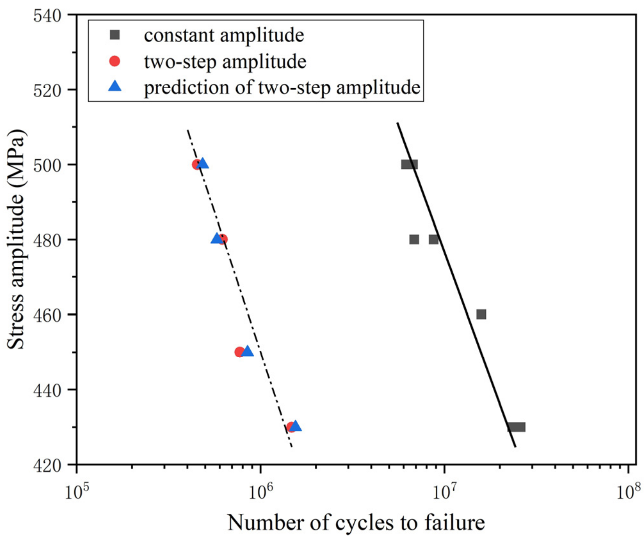


**Figure 7.** Comparison of the prediction of cumulative life and experimental data for the stress block with the second level of 2 × $10^5$ cycles.

### 3.2.3. Fatigue Damage Analysis

Cumulative fatigue damage of stress blocks with different stress was performed based on the fatigue damage model, as shown in Figure 8. In the case of the high stress for 10 cycles with 450 MPa/2 × $10^5$ cycles, fatigue damage of stress blocks increased with the increase in the high stress. When the high stress amplitude was increased to 950 MPa close to the yield strength, the stress block damage was significantly higher than that of 900 MPa and 850 MPa. As for the low stress for 2 × $10^5$ cycles with 950 MPa/10 cycles, fatigue damage of stress blocks increased with the increase in the number of stress blocks. The higher the second level stress amplitude, the faster the fatigue damage rate of the stress block.

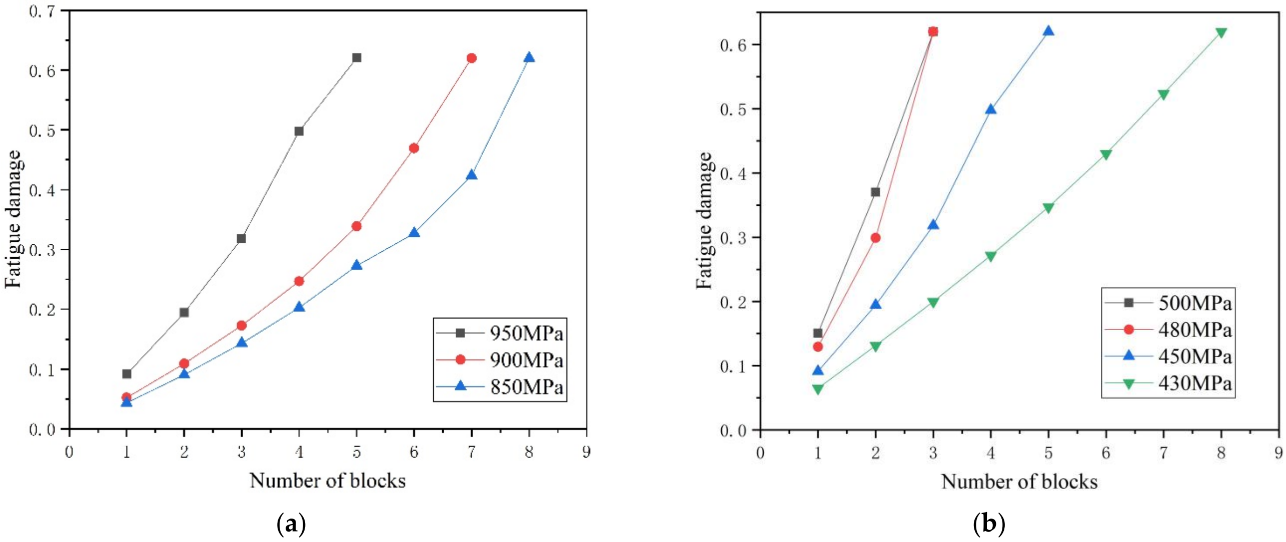


**Figure 8.** Effect of the stress level on fatigue damage of stress block: (**a**) the high stress for 10 cycles with 450 MPa/2 × $10^5$ cycles; and (**b**) the low stress for 2 × $10^5$ cycles with 950 MPa/10 cycles.

Figure 9 shows the cumulative fatigue damage of stress blocks with the different cycle numbers. In order to investigate the cycle number effect of the high stress block, the fatigue damage with 950 MPa for 10 cycles and 5 cycles was analyzed based on the damage model. According to Formulas (4) and (7), cumulative fatigue damage increased significantly with the increase in cycle ratio $N_i/N_R$ under constant stress amplitude. Figure 9a shows that stress blocks with 950 Pa/10 cycles obtained the highest cumulative fatigue damage due to the high stress amplitude, and the cumulative damage was almost linear with the number of cycle blocks due to the high stress. For stress blocks with 450 MPa/2 × $10^5$ cycles, fatigue cumulative damage was almost the same as that with 950 MPa/5 cycles in the first three stress blocks, and then significantly increased with the increase in cumulative cycles owing to its nonlinear damage. In consequence, fatigue damage was dramatically higher than that with 950 MPa/5 cycles. The cumulative fatigue damage of 450 MPa/2 × $10^4$ cycles was very small. According to Formulas (4) and (7), cumulative fatigue damage increased significantly with the increase in cycle ratio $N_i/N_R$. Thus, the small fatigue damage of 450 MPa/2 × $10^4$ cycles was attributed to the low cyclic ratio. Figure 9b shows that fatigue damage of stress blocks with 950 MPa/10 cycles and 450 MPa/2 × $10^5$ cycles was remarkably higher than that of 450 MPa/2 × $10^5$ cycles, indicating that the high stress accelerated fatigue damage of low stress.

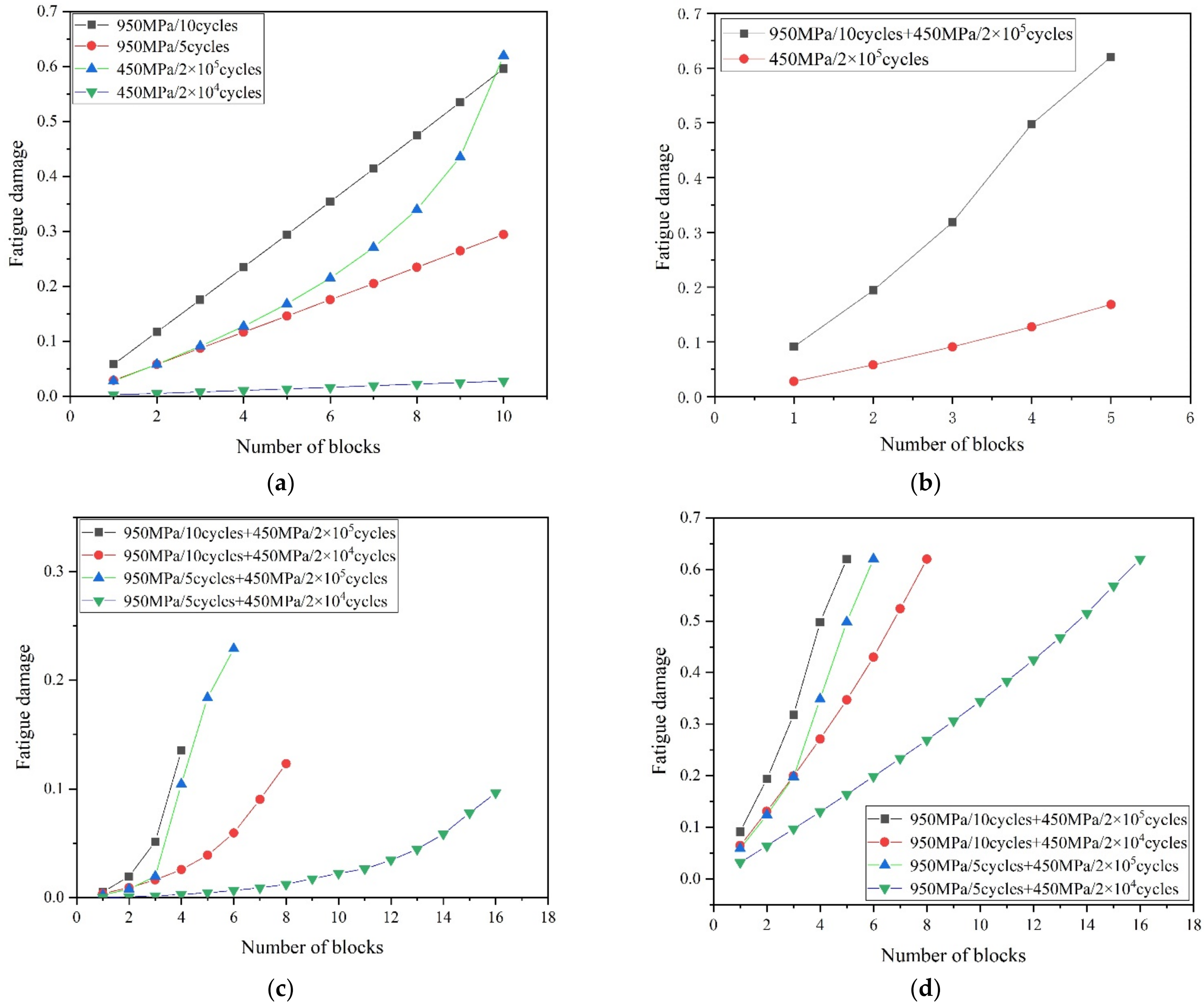


**Figure 9.** (**a**) Fatigue damage under constant amplitude loading; (**b**) comparison of stress blocks and low stress fatigue damage; (**c**) the interaction fatigue damage in different stress block; and (**d**) the total cumulative fatigue damage.

According to Formula (9), the interaction fatigue damage in different stress block is shown in Figure 9c. The interaction damage between 450 MPa/2 $\times$ $10^5$ cycles and 950 MPa stress was significantly larger than that of the stress block with 450 MPa/2 $\times$ $10^4$ cycles. As the number of cycles ratio $N_i/N_R$ for 450 MPa/2 $\times$ $10^5$ cycles was 10 times that of 2 $\times$ $10^4$ cycles, fatigue damage of stress blocks with 450 MPa/2 $\times$ $10^5$ cycles obtained a higher fatigue damage rate. Under the same initial fatigue damage, stress blocks with 450 MPa/2 $\times$ $10^5$ cycles acquired greater fatigue damage, illustrating the strong stress interaction. The stress blocks with 950 MPa/10 cycles and 450 MPa/2 $\times$ $10^5$ cycles gained the largest total fatigue damage, while stress blocks with 950 MPa/5 cycles and 450 MPa/2 $\times$ $10^4$ cycles obtained the lowest one. The total fatigue damage of stress blocks with 950 MPa/5 cycles and 450 MPa/2 $\times$ $10^5$ cycles was higher than that with 950 MPa/10 cycles and 450 MPa/2 $\times$ $10^4$ cycles (Figure 9d). Therefore, the cumulative fatigue damage of the stress blocks was related to the stress amplitude and the cycle ratio, which determined the stress fatigue damage and its interaction damage.

Comparison of stress blocks and LCF predamage fatigue damage is shown in Figure 10. Fatigue damage of LCF predamage specimens increased slowly under 450 MPa stress amplitude, and rapidly increased when reaching the critical damage value, where cracks initiated at the specimen subsurface [23]. The fatigue damage rate of stress blocks with 950 MPa/10 cycles and 450 MPa/2 $\times$ $10^5$ cycles was much higher than that of LCF predamage, and the high stress in stress blocks promoted the surface crack initiation. Fatigue damage at the third cycle block reached that of fatigue predamage, and was then higher than that of fatigue predamage. Thus, the cumulative life under the stress block was lower than of fatigue predamage. However, if cracks in the stress block were initiated at the specimen subsurface, fatigue damage decreased due to the large value of $B_0$ [17], and the cumulative life of 450 MPa stress amplitude was close to that of fatigue predamage. Therefore, the surface crack initiation of the stress block accelerated fatigue damage of low stress amplitude and significantly reduced the cumulative life of low stress amplitude.

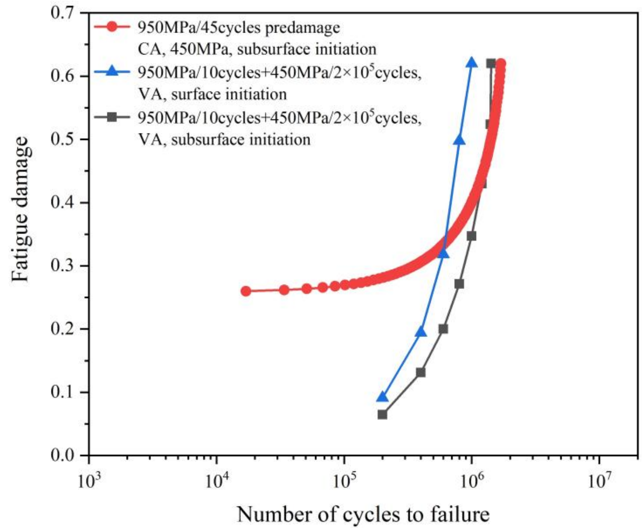


**Figure 10.** Comparison of stress blocks and LCF predamage fatigue damage.

## 4. Conclusions

(1) The high/low stress block significantly reduced the cumulative fatigue life of low stress amplitude, and the fatigue crack initiation site changed from the specimen subsurface under constant loading to the specimen surface under stress block.

(2) Based on continuum damage mechanics, fatigue damage models of two-step stress blocks were established to estimate the fatigue damage process. The prediction of cumulative fatigue life generally agreed with the experimental data with the error within 10%. Higher stress amplitude obtained greater stress fatigue damage and interaction damage. The surface crack initiation in the stress block accelerated fatigue damage of low stress amplitude, reducing the cumulative life.

**Author Contributions:** Z.Z. and D.C. conceived and designed the research; S.L., Y.W., Y.S., H.Q. and B.S. performed the experiment; B.N. analyzed and wrote the manuscript. All authors have read and agreed to the published version of the manuscript.

**Funding:** This research was funded by R and D plan for key areas in Guangdong Province (2020B010186001), Science and Technology Program of the Ministry of Science and Technology (G2022030060L), Core technology research project of Foshan (1920001000412), Basic and applied basic research fund project in Guangdong Province (2020b15120093), R and D plan for key areas in Jiangxi Province (20201BBE51009, 20212BBE51012), Foshan Material Computing Engineering Technology Research Center, Innovation driven project of science and technology plan in Jiangxi Yichun.

**Data Availability Statement:** The data presented in this study are available on request from the corresponding author.

**Conflicts of Interest:** The authors declare no conflict of interest.

## References


1. Zhao, Q.; Sun, Q.; Xin, S.; Chen, Y.; Wu, C.; Wang, H.; Xu, J.; Wan, M.; Zeng, W.; Zhao, Y. High-strength titanium alloys for aerospace engineering applications: A review on melting-forging process. *Mater. Sci. Eng. A* **2022**, *845*, 143260. [CrossRef]
2. Dantas, R.; Correia, J.; Lesiuk, G.; Rozumek, D.; Zhu, S.-P.; de Jesus, A.; Susmel, L.; Berto, F. Evaluation of multiaxial high-cycle fatigue criteria under proportional loading for S355 steel. *Eng. Fail. Anal.* **2021**, *120*, 105037. [CrossRef]
3. Singla, A.K.; Singh, J.; Sharma, V.; Gupta, M.; Song, Q.; Rozumek, D.; Królczyk, G.M. Impact of cryogenic treatment on HCF and FCP performance of β-solution treated Ti-6Al-4V ELI biomaterial. *Materials* **2020**, *13*, 500. [CrossRef] [PubMed]
4. Gao, T.; Xue, H.; Sun, Z.; Retraint, D.; He, Y. Micromechanisms of crack initiation of a Ti-8Al-1Mo-1V alloy in the very high cycle fatigue regime. *Int. J. Fatigue* **2021**, *150*, 106314. [CrossRef]
5. Sun, J.; Peng, W.; Sun, C. Mechanism of artificial surface defect induced cracking for very high cycle fatigue of Ti alloys. *Eng. Fract. Mech.* **2022**, *272*, 108721. [CrossRef]
6. Gao, T.; Xue, H.; Sun, Z.; Retraint, D. Investigation of crack initiation mechanism of a precipitation hardened TC11 titanium alloy at very high cycle fatigue loading. *Mater. Sci. Eng. A* **2020**, *776*, 138989. [CrossRef]
7. Liu, F.; Peng, H.; Liu, Y.; Wang, C.; Wang, Q.; Chen, Y. Crack initiation mechanism of titanium alloy in very high cycle fatigue regime at 400 °C considering stress ratio effect. *Int. J. Fatigue* **2022**, *163*, 107012. [CrossRef]
8. Li, C.; Li, W.; Cai, L.; Zhang, Y.; Sun, R.; Li, X.; Wang, P. Microstructure based cracking behavior and life assessment of titanium alloy at very-high-cycle fatigue with elevated temperatures. *Int. J. Fatigue* **2022**, *161*, 106914. [CrossRef]
9. Liu, F.; Chen, Y.; He, C.; Li, L.; Wang, C.; Li, H.; Liu, Y. Tensile and very high cycle fatigue behaviors of a compressor blade titanium alloy at room and high temperatures. *Mater. Sci. Eng. A* **2021**, *811*, 141049. [CrossRef]
10. Mayer, H. Fatigue damage of low amplitude cycles in low carbon steel. *J. Mater. Sci.* **2009**, *44*, 4919–4929. [CrossRef]
11. Fitzka, M.; Mayer, H. Constant and variable amplitude fatigue testing of aluminum alloy 2024-T351 with ultrasonic and servo-hydraulic equipment. *Int. J. Fatigue* **2016**, *91*, 363–372. [CrossRef]
12. Mayer, H.; Haydn, W.; Schuller, R.; Issler, S.; Bacher-Höchst, M. Very high cycle fatigue properties of bainitic high carbon–chromium steel under variable amplitude conditions. *Int. J. Fatigue* **2009**, *31*, 1300–1308.
13. Schönbauer, B.M.; Fitzka, M.; Karr, U.; Mayer, H. Variable amplitude very high cycle fatigue of 17-4PH steel with a stepwise SN curve. *Int. J. Fatigue* **2021**, *142*, 105963.
14. Li, G.; Ke, L.; Peng, W.; Ren, X.; Sun, C. Effects of natural aging and variable loading on very high cycle fatigue behavior of a bearing steel GCr15. *Theor. Appl. Fract. Mech.* **2022**, *119*, 103360. [CrossRef]
15. Hu, Y.; Sun, C.; Hong, Y. Crack growth rates and microstructure feature of initiation region for very-high-cycle fatigue of a high-strength steel. *Fatigue Fract. Eng. Mater. Struct.* **2018**, *41*, 1717–1732. [CrossRef]
16. Sun, C.; Song, Q.; Zhou, L.; Pan, X. Characteristic of interior crack initiation and early growth for high cycle and very high cycle fatigue of a martensitic stainless steel. *Mater. Sci. Eng. A* **2019**, *758*, 112–120. [CrossRef]
17. Song, Q.; Sun, C. Mechanism of crack initiation and early growth of high strength steels in very high cycle fatigue regime. *Mater. Sci. Eng. A* **2020**, *771*, 138648. [CrossRef]
18. Stäcker, C.; Sander, M. Experimental, analytical and numerical analyses of constant and variable amplitude loadings in the very high cycle fatigue regime. *Theor. Appl. Fract. Mech.* **2017**, *92*, 394–409. [CrossRef]
19. Sander, M.; Müller, T.; Lebahn, J. Influence of mean stress and variable amplitude loading on the fatigue behaviour of a high-strength steel in VHCF regime. *Int. J. Fatigue* **2014**, *62*, 10–20. [CrossRef]
20. Ritz, F.; Stäcker, C.; Beck, T.; Sander, M. FGA formation mechanism for X10CrNiMoV12-2-2 and 34CrNiMo6 for constant and variable amplitude tests under the influence of applied mean loads. *Fatigue Fract. Eng. M.* **2018**, *41*, 1576–1587. [CrossRef]
21. Zheng, Y.; Zhao, Z.; Zhang, Z.; Zong, W.; Dong, C. Internal crack initiation characteristics and early growth behaviors for very-high-cycle fatigue of a titanium alloy electron beam welded joints. *Mater. Sci. Eng. A* **2017**, *706*, 311–318. [CrossRef]
22. Nie, B.; Zhao, Z.; Ouyang, Y.; Chen, D.; Chen, H.; Sun, H.; Liu, S. Effect of low cycle fatigue predamage on very high cycle fatigue behavior of TC21 titanium alloy. *Materials* **2017**, *10*, 1384. [CrossRef] [PubMed]
23. Nie, B.; Liu, S.; Wu, Y.; Song, Y.; Qi, H.; Shi, B.; Zhao, Z.; Chen, D. Cumulative damage in very high/low cycle combined fatigue for TC21 titanium alloy. *Crystals* **2022**, *12*, 1702. [CrossRef]
24. Huang, Z.Y.; Wanger, D.; Bathias, C.; Chaboche, J.L. Cumulative fatigue damage in low cycle fatigue and gigacycle fatigue for low carbon-manganese steel. *Int. J. Fatigue* **2011**, *33*, 115–123. [CrossRef]
25. Huang, Z.Y.; Wang, Q.Y.; Wagner, D.; Bathias, C. Effect of low cycle fatigue predamage on very high cycle fatigue. *Theor. Appl. Mech. Lett.* **2012**, *2*, 031007. [CrossRef]
26. Nie, B.; Song, Y.; Huang, X.; Qi, H.; Zhao, Z.; Chen, D. Low cycle fatigue behavior of TC21 titanium alloy with bi-Lamellar basketweave microstructure. *Crystals* **2022**, *12*, 796. [CrossRef]
27. Bathias, C. Piezoelectric fatigue testing machines and devices. *Int. J. Fatigue* **2006**, *28*, 1438–1445. [CrossRef]
28. Nie, B.; Liu, S.; Huang, X.; Qi, H.; Shi, B.; Zhao, Z.; Chen, D. Low cycle fatigue crack damage behavior of TC21 titanium alloy with basketweave microstructure. *Crystals* **2022**, *12*, 1211. [CrossRef]